

Impact of $Al_xGa_{1-x}N$ barrier thickness and Al composition on electrical properties of ferroelectric HfZrO/Al_2O_3/AlGaN/GaN MFSHEMTs

Yue Li(李跃), Xingpeng Liu(刘兴鹏), Tangyou Sun(孙堂友), Fabi Zhang(张法碧), Tao Fu(傅涛), Peihua Wang-yang(王阳培华), Haiou Li(李海鸥), and Yonghe Chen(陈永和)

Citation: Chin. Phys. B, 2022, 31 (**9**): 097307. DOI: 10.1088/1674-1056/ac7b1a
Journal homepage: http://cpb.iphy.ac.cn; http://iopscience.iop.org/cpb

What follows is a list of articles you may be interested in

Improved device performance of recessed-gate AlGaN/GaN HEMTs by using *in-situ* N_2O radical treatment

Xinchuang Zhang(张新创), Mei Wu(武玫), Bin Hou(侯斌), Xuerui Niu(牛雪锐), Hao Lu(芦浩), Fuchun Jia(贾富春), Meng Zhang(张濛), Jiale Du(杜佳乐), Ling Yang(杨凌), Xiaohua Ma(马晓华), and Yue Hao(郝跃)

Chin. Phys. B, 2022, 31 (**5**): 057301. DOI: 10.1088/1674-1056/ac48fb

Extrinsic equivalent circuit modeling of InP HEMTs based on full-wave electromagnetic simulation

Shi-Yu Feng(冯识谕), Yong-Bo Su(苏永波), Peng Ding(丁芃), Jing-Tao Zhou(周静涛), Song-Ang Peng(彭松昂), Wu-Chang Ding(丁武昌), and Zhi Jin(金智)

Chin. Phys. B, 2022, 31 (**4**): 047303. DOI: 10.1088/1674-1056/ac2b1d

High power-added-efficiency AlGaN/GaN HEMTs fabricated by atomic level controlled etching

Xinchuang Zhang(张新创), Bin Hou(侯斌), Fuchun Jia(贾富春), Hao Lu(芦浩), Xuerui Niu(牛雪锐), Mei Wu(武玫), Meng Zhang(张濛), Jiale Du(杜佳乐), Ling Yang(杨凌), Xiaohua Ma(马晓华), and Yue Hao(郝跃)

Chin. Phys. B, 2022, 31 (**2**): 027301. DOI: 10.1088/1674-1056/ac1414

Protection of isolated and active regions in AlGaN/GaN HEMTs using selective laser annealing

Mingchen Hou(侯明辰), Gang Xie(谢刚), Qing Guo(郭清), and Kuang Sheng(盛况)

Chin. Phys. B, 2021, 30 (**9**): 097302. DOI: 10.1088/1674-1056/abf34c

Ferroelectric effect and equivalent polarization charge model of $PbZr_{0.2}Ti_{0.8}O_3$ on AlGaN/GaN MIS-HEMT

Yao-Peng Zhao(赵垚澎), Chong Wang(王冲), Xue-Feng Zheng(郑雪峰), Xiao-Hua Ma(马晓华), Ang Li(李昂), Kai Liu(刘凯), Yun-Long He(何云龙), Xiao-Li Lu(陆小力) and Yue Hao(郝跃)

Chin. Phys. B, 2021, 30 (**5**): 057302. DOI: 10.1088/1674-1056/abd469

Impact of $Al_xGa_{1-x}N$ barrier thickness and Al composition on electrical properties of ferroelectric HfZrO/Al_2O_3/AlGaN/GaN MFSHEMTs

Yue Li(李跃), Xingpeng Liu(刘兴鹏), Tangyou Sun(孙堂友), Fabi Zhang(张法碧), Tao Fu(傅涛), Peihua Wang-yang(王阳培华), Haiou Li(李海鸥)[†], and Yonghe Chen(陈永和)[‡]

Guangxi Key Laboratory of Precision Navigation Technology and Application, Guilin University of Electronic Technology (GUET), Guilin 541004, *China*

(Received 6 April 2022; revised manuscript received 2 June 2022; accepted manuscript online 22 June 2022)

Ferroelectric (FE) HfZrO/Al_2O_3 gate stack AlGaN/GaN metal-FE-semiconductor heterostructure high-electron mobility transistors (MFSHEMTs) with varying $Al_xGa_{1-x}N$ barrier thickness and Al composition are investigated and compared by TCAD simulation with non-FE HfO_2/Al_2O_3 gate stack metal–insulator–semiconductor heterostructure high-electron mobility transistors (MISHEMTs). Results show that the decrease of the two-dimensional electron gas (2DEG) density with decreasing AlGaN barrier thickness is more effectively suppressed in MFSHEMTs than that in MISHEMTs due to the enhanced FE polarization switching efficiency. The electrical characteristics of MFSHEMTs, including transconductance, subthreshold swing, and on-state current, effectively improve with decreasing AlGaN thickness in MFSHEMTs. High Al composition in AlGaN barrier layers that are under 3-nm thickness plays a great role in enhancing the 2DEG density and FE polarization in MFSHEMTs, improving the transconductance and the on-state current. The subthreshold swing and threshold voltage can be reduced by decreasing the AlGaN thickness and Al composition in MFSHEMTs, affording favorable conditions for further enhancing the device.

Keywords: ferroelectric polarization, HfZrO, ferroelectric gate, HEMTs

PACS: 73.40.Kp, 73.40.Qv, 77.90.+k **DOI:** 10.1088/1674-1056/ac7b1a

1. Introduction

Due to the considerable two-dimensional electron gas (2DEG) and large bandgap present in AlGaN/GaN heterostructures, GaN metal–oxide–semiconductor high-electron mobility transistors have attracted significant attention in radio frequency and power applications.[1–4] Conventional gate oxide dielectric layers cause the degradation of transconductance and the overall gate capacitance density.[5–7] To solve this problem, ferroelectric oxide as a gate insulator is employed because of the high dielectric constant and negative capacitance (NC) effect.[8–10] Conventional perovskite-type FE materials, such as $PbZrTiO_3$,[11–13] $BaTiO_3$,[14,15] and $SrTiO_3$,[16–19] have some distinct disadvantages for complementary metal–oxide–semiconductor (CMOS) compatibility because of the FE properties of the unstable ultra-thin films. Based on the compatible CMOS technology, FE HfO_2-based films, such as $HfZrO_2$,[20–22] $HfAlO_2$,[23–25] $HfYO_2$,[26–28] and $HfLaO_2$,[29–31] have become attractive candidates through atomic layer deposition (ALD) technology. An FE HfZrO film can exhibit higher FE polarization at low deposition temperatures in HfO_2-based films.[32] However, a poor interface between a GaN high-electron mobility transistor (HEMT) and an FE HfZrO film causes the degradation of the FE and electrical properties. To realize a high interface quality, a buffer layer such as Si_3N_4 and Al_2O_3,[33–36] is introduced between FE gate dielectrics and AlGaN/GaN heterostructures. Owing to the wide band gap of Al_2O_3, it plays an important role in suppressing the gate leakage current. Moreover, Al_2O_3 as the buffer dielectric layer is near thickness of 1.6 nm for TiN/HfZrO/Al_2O_3/TiN capacitors,[37] and the FE properties of HfZrO films are thus improved, providing an approach for integrating FE HfZrO thin films in GaN HEMTs.

NC field-effect transistors have been realized for Si and Ge substrates due to the polarization switching of FE materials, improving the subthreshold swing (*SS*) and transconductance (G_m).[38,39] Based on the NC effect of FE materials, obtaining a high density of 2DEG from AlGaN/GaN heterostructures is still difficult.[40] The polarization of the AlGaN layer causes the pinning effect of the FE dipole self-alignment, and the direction of FE polarization remains consistent with the direction of the AlGaN barrier layer even after the poling operation,[41] which hinder FE polarization switching efficiency. Additionally, the dielectric constant of an FE film is considerably higher than that of the AlGaN layer. Thus, part of the voltage is applied to the AlGaN layer, which weakens the FE polarization. In this work, the impact of the $Al_xGa_{1-x}N$ thickness and Al composition on the electrical properties of FE heterostructure HfZrO/Al_2O_3/AlGaN/GaN MFSHEMTs are investigated by using TCAD simulation. Based on ferroelectric polarization theory and device structure analysis, a phys-

[†]Corresponding author. E-mail: lihaiou@guet.edu.cn
[‡]Corresponding author. E-mail: yhchen@guet.edu.cn

© 2022 Chinese Physical Society and IOP Publishing Ltd

ical model of the device is constructed. The theoretical relationship between FE polarization-induced 2DEG distribution and conduction band is discussed. Compared to the non-FE device, we optimized the thickness of AlGaN barrier and the composition of AlGaN to improve FE polarization and 2DEG in MFSHEMTs, and the electrical characteristics of G_m, SS, and I_{on} can be enhanced due to the improvement of the FE layer.

2. Device structure and simulation model

A 12-nm $Hf_{0.5}Zr_{0.5}O_2$/1-nm Al_2O_3 FE dielectric layer was deposited by ALD on TiN/Pt/Si substrates at 250 °C using tetrakis(ethylmethylamino)hafnium, tetrakis(dimethylamino)zirconium, trimethylaluminum, and deionized water (H_2O) as the Hf precursor, Zr precursor, Al precursor, and oxygen source, respectively. Next, a TiN top electrode was grown using direct current sputtering. Finally, a TiN/$Hf_{0.5}Zr_{0.5}O_2$/Al_2O_3/TiN FE capacitor was annealed in ambient N_2 atmosphere at 450 °C for 30 s. Remnant polarization (P_r) of 18.5 μC/cm^2 and a coercive electric field (E_c) of 1.25 V were measured using TF analyzer 2000 (Aixacct systems). To describe the NC effect of an FE $Hf_{0.5}Zr_{0.5}O_2$/Al_2O_3 capacitor in simulation, the Landau–Khalatnikov (LK) model is considered by[8,42,43]

$$E_{FE} = 2\alpha P_{FE} + 4\beta P_{FE}^3 + 6\gamma P_{FE}^5, \tag{1}$$

where P_{FE} is the polarization and α, β, and γ are the LK parameters for the FE film. The P–V simulation curve of the $Hf_{0.5}Zr_{0.5}O_2$/Al_2O_3 capacitor fit the experimental results in Fig. 1. The α, β, and γ parameters are equal to -8.1×10^{10} cm/F, 4.5×10^{19} cm^5/(F·C^2), and 2×10^{28} cm^9/(F·C^4), respectively. Based on the obtained results, the FE characteristics of the $Hf_{0.5}Zr_{0.5}O_2$/Al_2O_3 films were used in the $Al_xGa_{1-x}N$/GaN MFSHEMT.

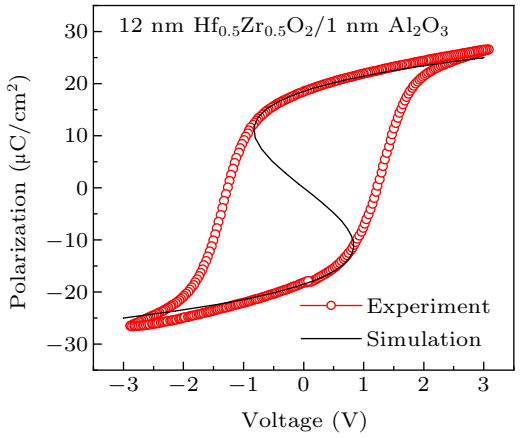


Fig. 1. The P–V characteristics of the $HfZrO_2$/Al_2O_3 capacitor. Symbols: The data obtained by the P–V measurement. Solid lines: P–V curve matched by the LK FE model.

Figure 2(a) displays the 2D schematic diagram of the $Al_xGa_{1-x}N$/GaN MFSHEMTs. The down–up epitaxy layer structures comprised the Si substrate, 3-μm GaN buffer layer, 50-nm GaN channel layer, 20-nm $Al_xGa_{1-x}N$ barrier layer, and 2-nm GaN cap layer. A 12-nm $Hf_{0.5}Zr_{0.5}O_2$/1-nm Al_2O_3 FE layer and a 12-nm HfO_2/1-nm Al_2O_3 non-FE layer were introduced as the gate stack of the $Al_xGa_{1-x}N$/GaN devices. The orthorhombic phase crystal structure of the HfZrO film was in a metastable state, and it did not match the lattice of the $Al_xGa_{1-x}N$ barrier layer, affording poor interface quality. The $Al_xGa_{1-x}N$ barrier layer and HfZrO film were separated by an Al_2O_3 inserting layer to yield better device reliability. The interface net charge of Al_2O_3/AlGaN was $+9.5\times10^{12}$ cm^{-2}.[44] For the $Al_xGa_{1-x}N$/GaN MISHEMTs, the gate length was 2 μm, gate–drain spacing was 5 μm, and gate–source distance was 3 μm. The thickness (T) of the $Al_xGa_{1-x}N$ layer under the gate stack were 20, 15, 10, 7, and 3 nm, respectively. In order to achieve the FE HfZrO/Al_2O_3 gate stack AlGaN/GaN heterostructure MFSHEMTs in simulation, drift-diffusion model to solve the Poisson's equation self-consistently with carrier continuity equation have been carried out using TCAD. Shockley–Read–Hall (SRH) model and Fermi–Dirac model are used in device simulation. Caughey–Thomas mobility model is considered to express the experimental values measured in the c-plane GaN,[45] including electron mobility μ = 1000 cm^2/V·s and hole mobility μ = 170 cm^2/V·s.

To analyze the effect of the Al composition in $Al_xGa_{1-x}N$ barrier layer with different thicknesses on the AlGaN polarization, the polarization analytical equations are provided.[46] For the FE/$Al_xGa_{1-x}N$/GaN MFSHEMTs, the piezoelectric equation can be expressed as

$$P_{pe}(\text{AlGaN}) = 2\times\varepsilon_{xx}\times\left(e_{31} - \frac{C_{13}\times e_{33}}{C_{33}}\right), \tag{2}$$

$$\varepsilon_{xx} = \varepsilon_{yy} = \frac{a_{GaN} - a_{AlGaN}}{a_{AlGaN}}, \tag{3}$$

where e_{31} and e_{33} are the AlGaN strain–charge piezoelectric coefficients, C_{13} and C_{33} are the AlGaN stiffness constants, ε_{xx} and ε_{yy} are the lattice mismatch-induced strains, and a is the lattice constant. The spontaneous polarization in the $Al_xGa_{1-x}N$ layer is given by

$$P_{sp}(\text{AlGaN}) = P_{sp}(\text{AlN})\times x + P_{sp}(\text{GaN})\times(1-x), \tag{4}$$

where P_{sp} (AlN) and P_{sp} (GaN) are the spontaneous polarization vectors of the AlN and GaN crystals, respectively, and x represents the Al mole fraction in the AlGaN layer. The total polarization charge is induced by the piezoelectric and spontaneous polarization in Fig. 2(b). The following equations can be used:

$$\sigma_{AlGaN} = P_{pe}(\text{AlGaN}) + P_{sp}(\text{AlGaN}), \tag{5}$$

$$\sigma_{GaN} = P_{sp}(\text{GaN}), \tag{6}$$

$$\Delta\sigma_{AlGaN/GaN} = \sigma_{AlGaN} - \sigma_{GaN}, \tag{7}$$

where σ_{AlGaN} and σ_{GaN} are the piezoelectric and spontaneous polarization charges of the AlGaN and GaN crystals, respectively. $\Delta\sigma_{AlGaN/GaN}$ represents the total polarization charge of the $Al_xGa_{1-x}N$/GaN heterostructure. The total polarization charge and its Al composition are calculated using Eqs. (2)–(7), which are illustrated in Table 1. As shown in Table 1, the piezoelectric polarization value is about four times higher than that of the spontaneous polarization, indicating that the piezoelectric polarization is the dominant factor for the induced total polarization charge. Furthermore, the spontaneous polarization and piezoelectric polarization increase with the Al composition of the $Al_xGa_{1-x}N$/GaN heterostructure, which increases the 2DEG density. Based on this estimate, the $Al_xGa_{1-x}N$ polarization and polarized charge can be controlled by adjusting the Al composition.

Due to the control effect of the FE polarization in FE/$Al_xGa_{1-x}N$/GaN MFSHEMTs, the initial status of the FE dielectric layer must be considered. As shown in Fig. 2(b), the negative polarization charge ($\Delta\sigma_{NPC}$) comprises the FE polarization charge (σ_{FE}) and the AlGaN polarization-induced charge (σ_{AlGaN}):

$$\Delta\sigma_{NPC} = \sigma_{FE} - \sigma_{AlGaN}. \tag{8}$$

Since the FE polarization of the FE dielectric layer is affected under AlGaN polarization, the AlGaN polarization self-aligns the FE film dipole parallel to the AlGaN barrier layer polarization, affording a positive FE polarization charge (σ_{FE}) at the $Hf_{0.5}Zr_{0.5}O_2/Al_2O_3$ lower surface.

Table 1. Calculated polarization values in the $Al_xGa_{1-x}N$/GaN heterostructure.

$Al_xGa_{1-x}N$ (x)	P_{sp} (μC/cm^2)	P_{pe} (μC/cm^2)	$\Delta\sigma_{AlGaN/GaN}$ (μC/cm^2)
0.35	−4.72	−1.36	3.18
0.3	−4.46	−1.14	2.7
0.25	−4.2	−0.933	2.233
0.2	−3.94	−0.73	1.77
0.15	−3.68	−0.54	1.32
0	−2.9	–	–

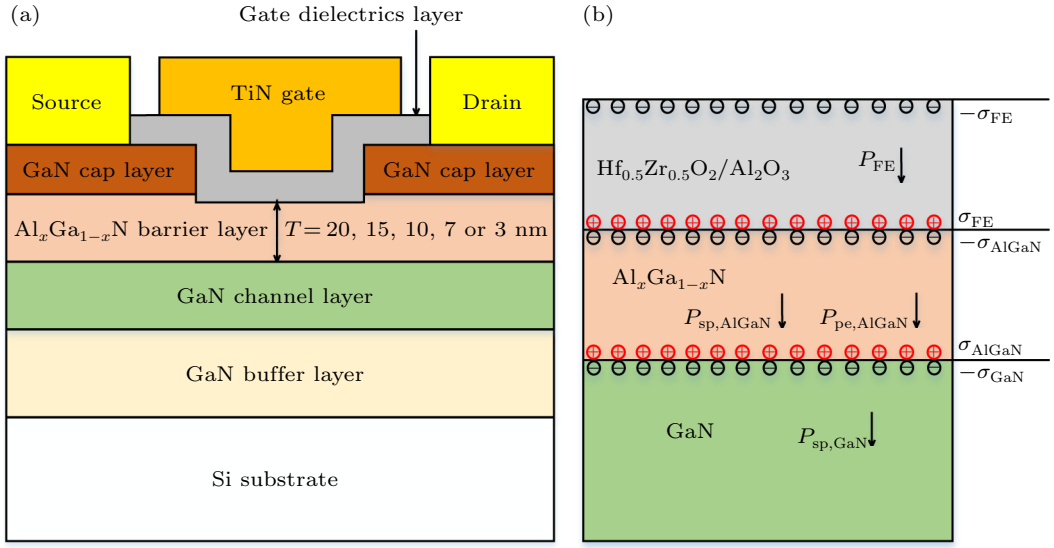


Fig. 2. (a) Schematic diagram of the device structure of the $Al_xGa_{1-x}N$/GaN MFSHEMT with an FE gate stack of $Hf_{0.5}Zr_{0.5}O_2/Al_2O_3$ and a non-FE gate stack of HfO_2/Al_2O_3. (b) Polarization effects of the FE/AlGaN/GaN structure with induced surface charge, including AlGaN spontaneous polarization (P_{sp}, AlGaN), AlGaN piezoelectric polarization (P_{pe},AlGaN,), GaN spontaneous polarization (P_{sp},GaN), and FE polarization (P_{FE}).

3. Results and discussion

HfZrO/Al_2O_3/AlGaN/GaN MFSHEMTs are investigated with varying $Al_xGa_{1-x}N$ thickness and Al composition in Figs. 3(a) and 3(b). Figure 3(a) presents the curves of the FE polarization in MFSHEMTs with varying $Al_{0.25}Ga_{0.75}N$ barrier layer thickness. The FE polarization of the HfZrO/Al_2O_3 FE film induces a positive FE polarization charge σ_{FE} that is oriented parallel to the AlGaN barrier layer polarization because of the pinning effect induced from the AlGaN polarization at the FE/AlGaN interface,[41] greatly weakening the controllability of the gate FE effect. With the thinning of the AlGaN barrier layer, the slope of FE polarization curves increases, subsequently enhancing the switching efficiency of the FE polarization. The polarization value of FE HfZrO/Al_2O_3 dielectrics layer increases with the increase of applied electric field. The polarization of AlGaN barrier layer hinders the increase of FE polarization at $V_g < 0.6$ V because of the pinning effect. When conduction band of AlGaN barrier layer is bent below the Fermi level at $V_g > 0.6$ V, electron concentration increases in the oxide/AlGaN interface. The electric field applied on FE HfZrO/Al_2O_3 dielectrics layer suddenly increases, leading to a sudden rise in FE polarization. The results indicate that electron concentration increase in the FE/AlGaN interface at $V_g > 0.6$ V, which increases the FE polarization.[37] The barrier height in the $Al_xGa_{1-x}N$/GaN heterostructure increases with the increasing Al composition

in the $Al_xGa_{1-x}N$ barrier layer, and a higher gate voltage is required to cause an abrupt increase of the FE polarization in Fig. 3(b).

In Fig. 4(a), we show the FE polarization of the $HfZrO/Al_2O_3/Al_xGa_{1-x}N/GaN$ capacitors with varying AlGaN barrier thickness and Al composition. With the thinning of the AlGaN barrier layer, the FE polarization of $HfZrO/Al_2O_3$ gate stack improves, especially at the high Al compositions. The negative polarization charge of AlGaN surface in different AlGaN barrier thicknesses are the same between FE $HfZrO/Al_2O_3/AlGaN/GaN$ and non-FE $HfO_2/Al_2O_3/AlGaN/GaN$ capacitors. Compared with non-FE $HfO_2/Al_2O_3/AlGaN/GaN$ capacitor, FE polarization charge of FE $HfZrO/Al_2O_3/AlGaN/GaN$ capacitor is increased by the thinning of the AlGaN barrier layer. According to the formula (8), the increase of the FE polarization with the thinning of the AlGaN barrier layer causes the reduction of the negative polarization charge density at the oxide/AlGaN interface in Fig. 4(b). Consequently, the AlGaN energy barrier reduces and the 2DEG in the channel increases in the FE $HfZrO/Al_2O_3/AlGaN/GaN$ capacitor compared with that in the non-FE HfO_2/Al_2O_3 gate stack in Figs. 5(a)–5(c). Furthermore, the 2DEG density of FE $HfZrO/Al_2O_3$ MFSHEMTs improves by 30.5%, 58.0%, and 134.3% compared to that of the non-FE HfO_2/Al_2O_3 gate stack with $Al_{0.25}Ga_{0.75}N$ barrier thicknesses of 20, 10, and 3 nm, respectively, indicating that the reduction of the 2DEG density is suppressed with the FE polarization enhancement. The 2DEG density distributions and conduction band profiles of the $HfZrO/Al_2O_3/Al_xGa_{1-x}N/GaN$ and $HfO_2/Al_2O_3/Al_xGa_{1-x}N/GaN$ structures with a 3-nm $Al_xGa_{1-x}N$ barrier thickness and Al compositions of 0.35, 0.2, and 0.15 are shown in Figs. 5(d)–5(e). The 2DEG density of the FE $HfZrO/Al_2O_3$ MFSHEMTs with the Al compositions of 0.35, 0.2, and 0.15 was 1.16×10^{13}, 4.9×10^{12}, and 2.81×10^{12} cm^{-2} at $V_{gs}=0$ V, representing an increase of 174%, 108%, and 95% than that of the non-FE HfO_2/Al_2O_3 gate stack, respectively. The 2DEG density of the FE $HfZrO/Al_2O_3$ MFSHEMTs with AlGaN barrier thickness of 3 nm can be improved by increasing the Al compositions.

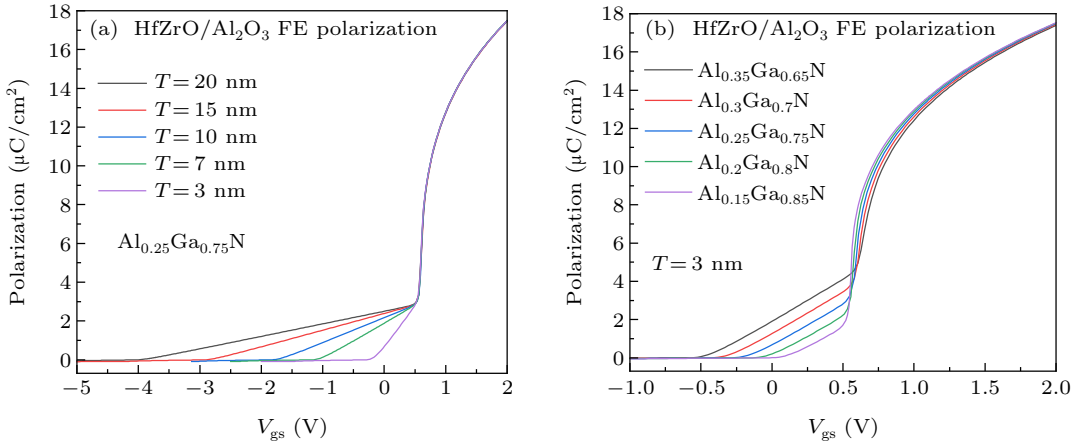


Fig. 3. (a) FE polarization of the $HfZrO/Al_2O_3/Al_{0.25}Ga_{0.75}N/GaN$ capacitors for $Al_{0.25}Ga_{0.75}N$ barrier thicknesses of 20, 15, 10, 7, and 3 nm. (b) FE polarization of the $HfZrO/Al_2O_3/Al_xGa_{1-x}N/GaN$ capacitors for the $Al_xGa_{1-x}N$ barrier thickness of 3 nm with Al compositions of 0.35, 0.3, 0.25, 0.2, and 0.15.

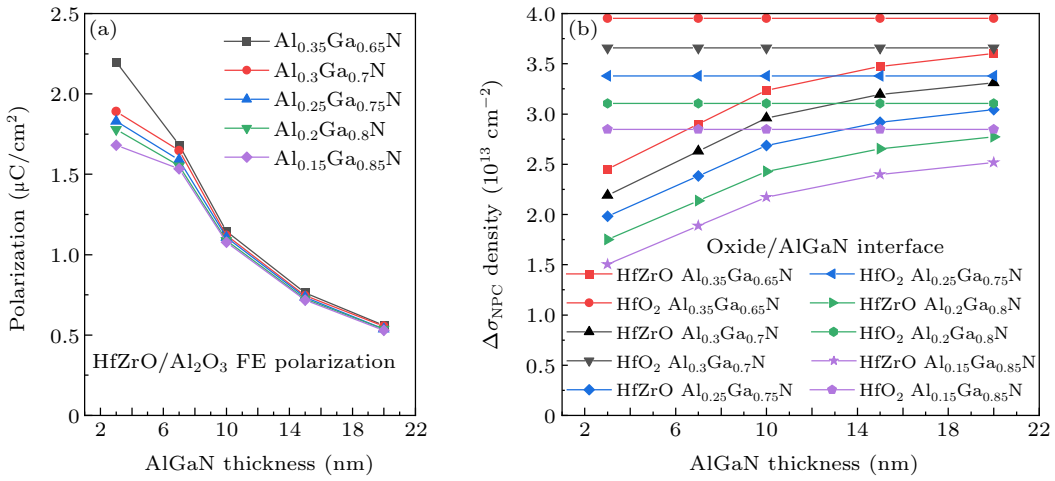


Fig. 4. (a) FE polarization of the $HfZrO/Al_2O_3/Al_xGa_{1-x}N/GaN$ capacitors and (b) $\Delta\sigma_{NPC}$ density of the oxide/AlGaN interface at $V_{gs}=V_{TH}+1$ V for the $Al_xGa_{1-x}N$ barrier thicknesses of 20, 15, 10, and 7 nm. When the $Al_xGa_{1-x}N$ barrier thickness is 3 nm, $V_{gs}=V_{TH}+0.5$ V.

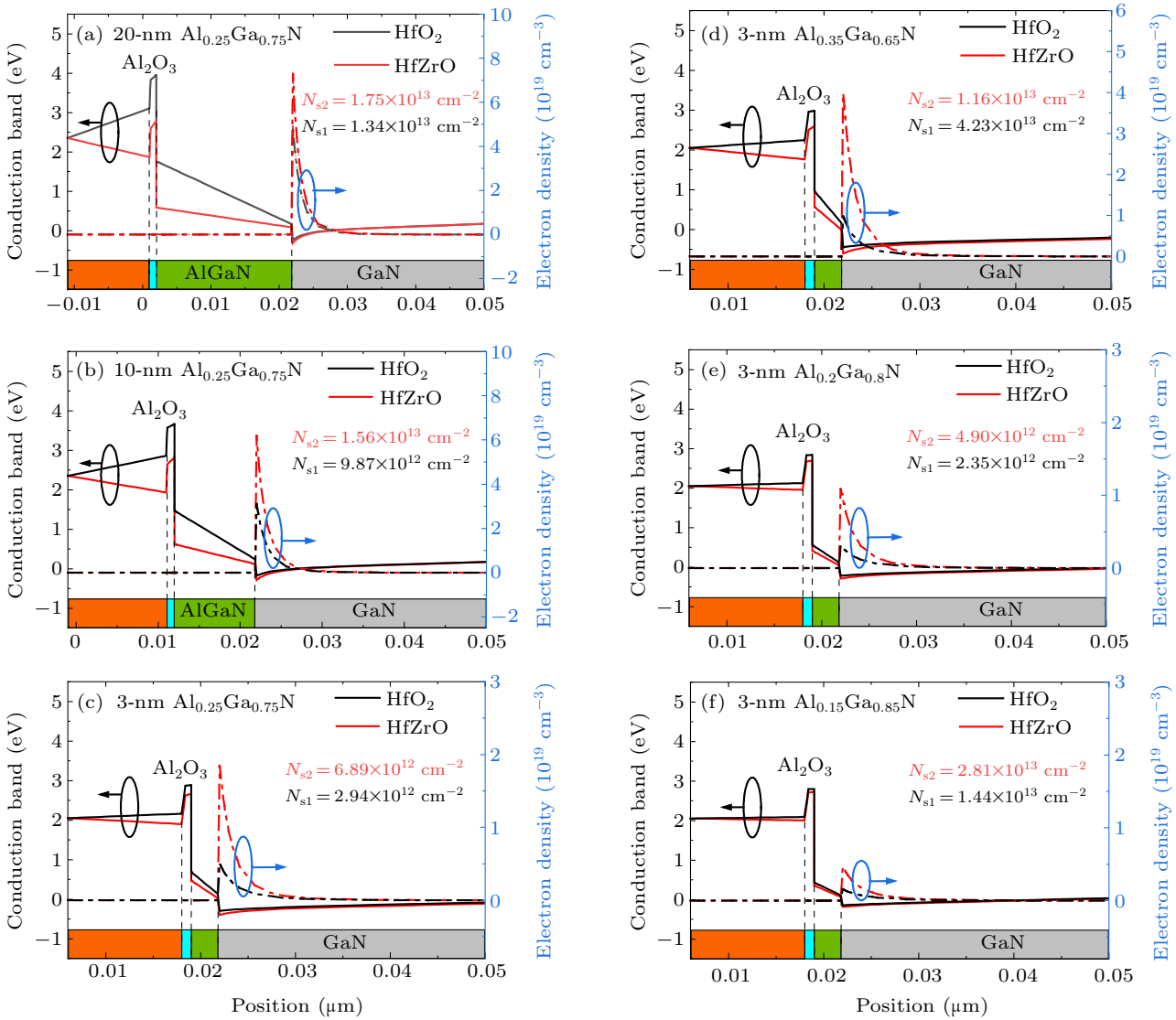


Fig. 5. The 2DEG density distribution and conduction band profiles of the HfZrO/Al_2O_3/$Al_{0.25}Ga_{0.75}N$/GaN and HfO_2/Al_2O_3/$Al_{0.25}Ga_{0.75}N$/GaN capacitors for AlGaN barrier thicknesses of 20 (a), 10 (b), and 3 nm (c). The 2DEG density distribution and conduction band profiles of the HfZrO/Al_2O_3/$Al_xGa_{1-x}N$/GaN and HfO_2/Al_2O_3/$Al_xGa_{1-x}N$/GaN capacitors for 3-nm AlGaN barrier thickness and Al compositions of 0.35 (d), 0.2 (e), and 0.15 (f). The gate voltage is 0 V.

To further evaluate the impact of the AlGaN barrier thickness and Al composition on MFSHEMTs, *C*–*V* and I_{ds}–V_{gs} curves are depicted in Figs. 6 and 7. For the AlGaN thicknesses of 20, 15, 10, 7, and 3 nm, the capacitance of FE HfZrO/Al_2O_3/$Al_{0.25}Ga_{0.75}N$/GaN structure exhibits an increase of 40.4%, 64.7%, 80.7%, 117.3%, and 285.7%, respectively, over that of the non-FE HfO_2/Al_2O_3 gate stack, as shown in Fig. 6(a). This is due to the improving FE polarization of the HfZrO/Al_2O_3 gate stack with the thinning of the AlGaN barrier layer in MFSHEMTs. Similarly, the drive current of FE HfZrO/Al_2O_3 MFSHEMTs with AlGaN thicknesses of 20, 15, 10, 7, and 3 nm increased by 6.4%, 10.7%, 21.7%, 26.3%, and 71.3%, respectively, compared to that of the non-FE HfO_2/Al_2O_3 gate stack, as shown in Fig. 6(b). The bulge in the capacitance curves at V_{gs} = 0.6 V is due to the increase of electron concentration in FE/AlGaN interface, which is consistent with the result in Fig. 3. These results suggest that the FE polarization effect of the HfZrO/Al_2O_3 gate stack plays a significant role in improving the electrical properties of MFSHEMTs based on the optimization of the AlGaN barrier thickness. The capacitance of the FE HfZrO/Al_2O_3/$Al_xGa_{1-x}N$/GaN structure with a 3-nm $Al_xGa_{1-x}N$ barrier thickness and Al compositions of 0.35, 0.3, 0.25, 0.2, and 0.15 was 3.14, 3.05, 3.00, 2.90, and 2.73 μC/cm^2, signifying improvements of 290.0%, 282.9%, 282.4%, 277.2%, and 267.4% than that of the non-FE HfO_2/Al_2O_3 gate stack in Fig. 7(a), respectively. This can be explained by the increase of the FE polarization with the Al composition when the $Al_xGa_{1-x}N$ barrier thickness is 3 nm. Thus, the drive current of the FE HfZrO/Al_2O_3 MFSHEMTs in the 3-nm $Al_xGa_{1-x}N$ barrier thinkness with the Al compositions of 0.35, 0.3, 0.25, 0.2, and 0.15, improves by 30.6%, 17.6%, 11.2%, 5.8%, and 5.1%, respectively, over that of non-FE HfO_2/Al_2O_3 gate stack in Fig. 7(b).

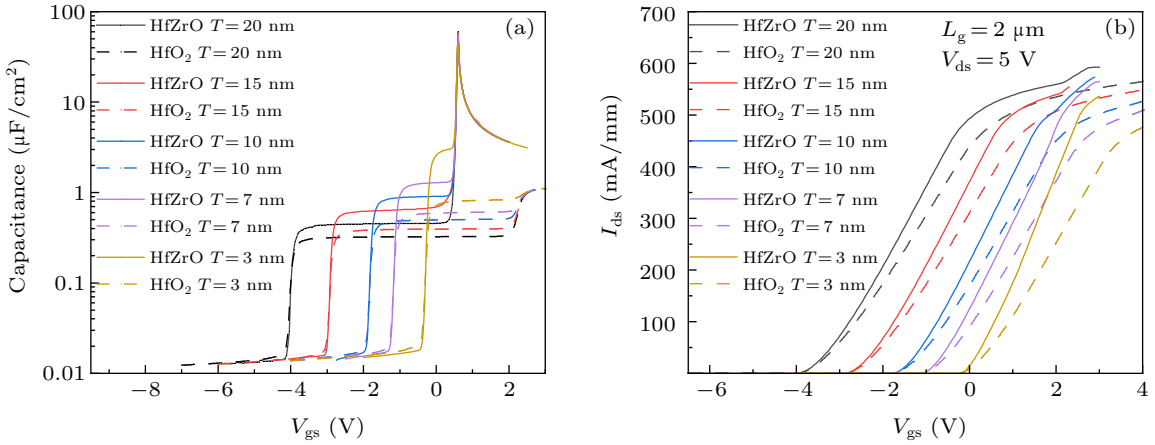


Fig. 6. (a) The *C*–*V* and (b) I_{ds}–V_{gs} curves of the HfZrO/Al_2O_3/$Al_{0.25}Ga_{0.75}N$/GaN MFSHEMT and HfO_2/Al_2O_3/$Al_{0.25}Ga_{0.75}N$/GaN MISHEMT for AlGaN barrier thicknesses of 20, 15, 10, 7, and 3 nm.

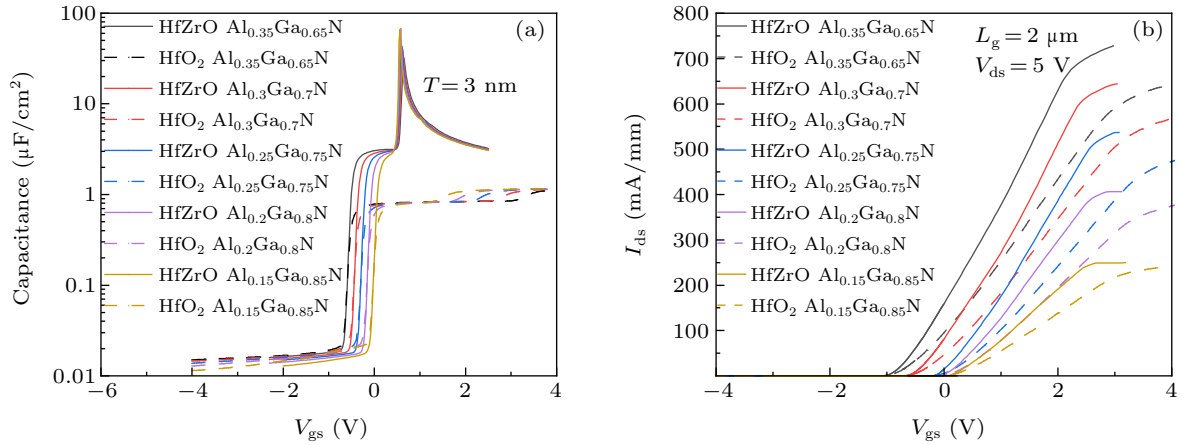


Fig. 7. (a) The *C*-*V* and (b) I_{ds}–V_{gs} curves of the HfZrO/Al_2O_3/$Al_xGa_{1-x}N$/GaN MFSHEMT and HfO_2/Al_2O_3/$Al_xGa_{1-x}N$/GaN MISHEMT for the 3-nm $Al_xGa_{1-x}N$ barrier thickness with Al compositions of 0.35, 0.3, 0.25, 0.2, and 0.15.

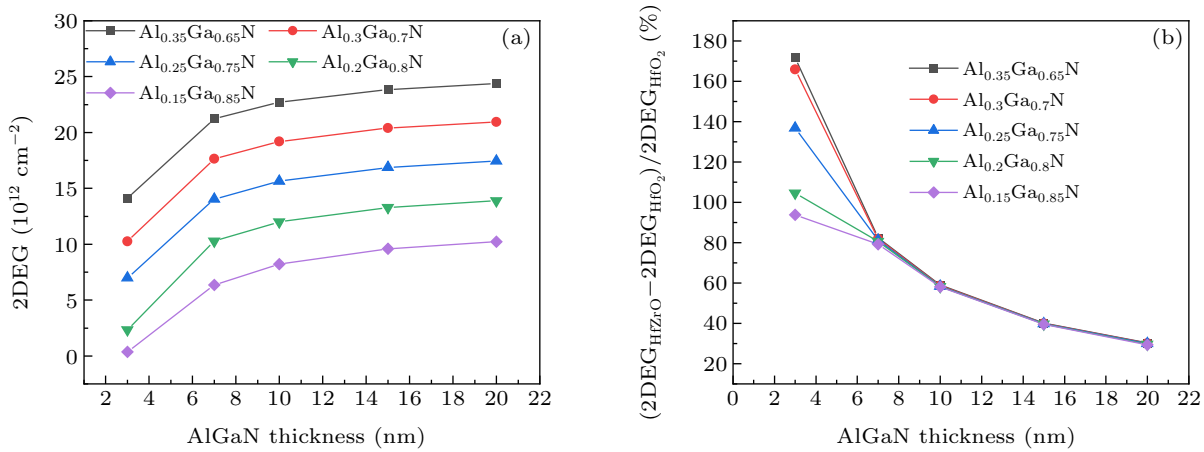


Fig. 8. (a) 2DEG density of the FE HfZrO/Al_2O_3/$Al_xGa_{1-x}N$/GaN capacitor and (b) the difference percentage of the 2DEG density based on FE HfZrO/Al_2O_3/$Al_xGa_{1-x}N$/GaN and non-FE HfO_2/Al_2O_3/$Al_xGa_{1-x}N$/GaN capacitors with varying AlGaN thickness and Al composition.

Figure 8(a) depicts the 2DEG density of the FE HfZrO/Al_2O_3/$Al_xGa_{1-x}N$/GaN structure with varying AlGaN barrier thickness and Al composition. When the thickness of the AlGaN layer decreased below 7 nm, the 2DEG density rapidly decreased. However, the reduction of 2DEG density was suppressed when the Al composition was increased. Therefore, to a certain extent, the decrease of the 2DEG density can be suppressed by increasing the Al composition with the thinning of AlGaN layer. To analyze the influence of the FE polarization under different Al compositions and $Al_xGa_{1-x}N$ layer thickness on the 2DEG density, the difference percentage of the 2DEG density $[(2DEG_{HfZrO}-2DEG_{HfO2})/2DEG_{HfO2}]$ was calculated for the FE and non-FE devices in Fig. 8(b). The difference percentage of the

2DEG density with different Al composition was close to 30%, 40%, 59%, and 82% with the AlGaN thicknesses of 20, 15, 10, and 7 nm, respectively. The difference percentage of 2DEG afforded by FE polarization with varying Al composition was basically the same under the same AlGaN thickness from 20 nm to 7 nm, which is consistent with the FE polarization of FE HfZrO/Al_2O_3 gate stack in Fig. 8(a). However, the difference percentage of the 2DEG density increased with the Al composition for the 3-nm $Al_xGa_{1-x}N$ barrier thickness. The 2DEG density of the 3-nm $Al_xGa_{1-x}N$ barrier thickness with varying Al composition exhibits an enormous difference due to the FE polarization of the FE HfZrO/Al_2O_3 gate stack and polarization of the $Al_xGa_{1-x}N$ barrier layer, as shown in Figs. 4(a) and 5(d)–5(f). The results show that the reduction of 2DEG density can be suppressed by increasing the Al composition for a 3-nm $Al_xGa_{1-x}N$ barrier thickness in MFSHEMTs compared to that of the non-FE HfO_2/Al_2O_3 gate stack.

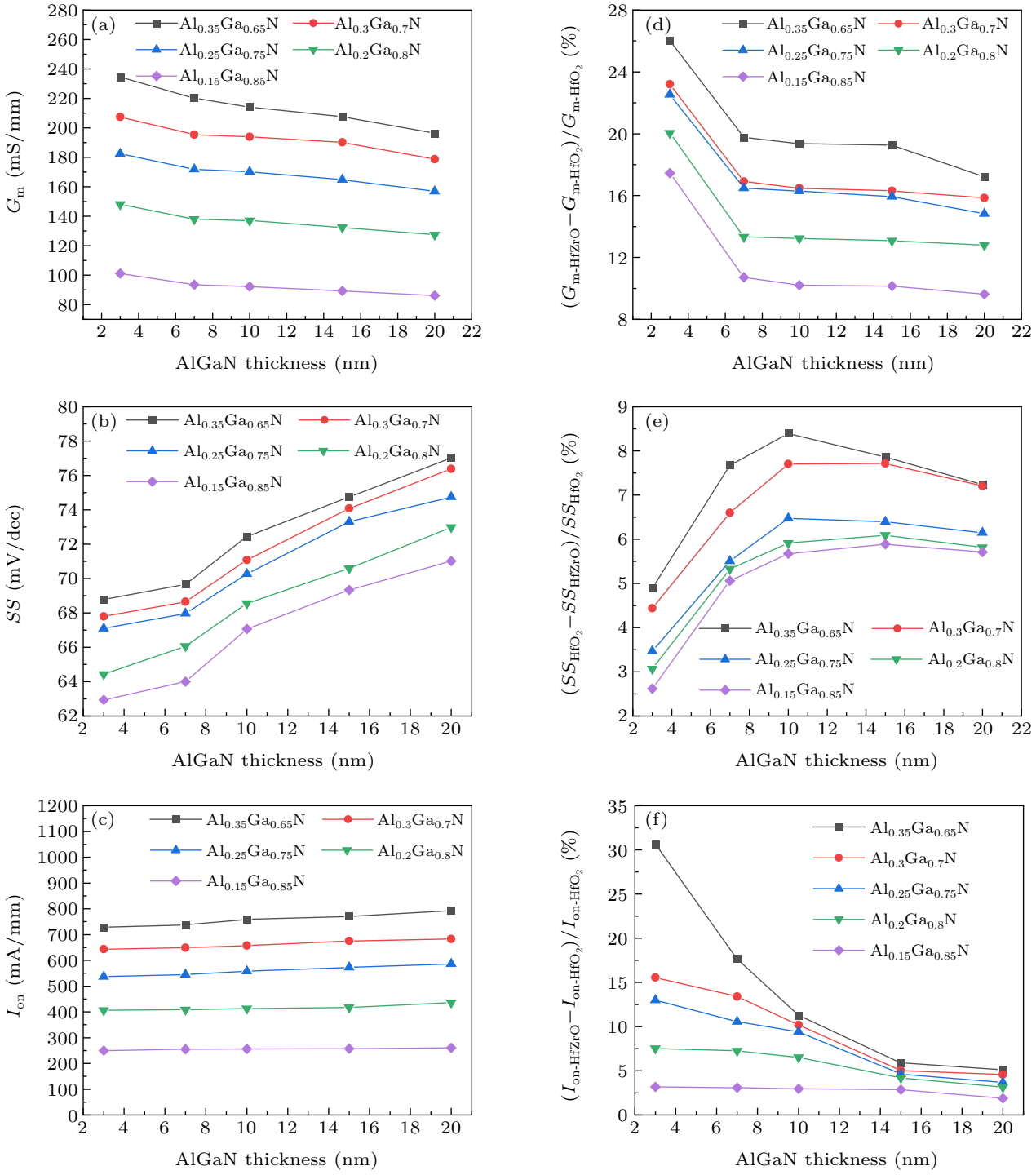


Fig. 9. (a) The G_m, (b) SS, and (c) I_{on} curves of FE HfZrO/Al_2O_3/$Al_xGa_{1-x}N$/GaN MFSHEMTs with varying $Al_xGa_{1-x}N$ thickness and Al composition. The difference percentage curves of (d) G_m, (e) SS, and (f) I_{on} based on the FE MFSHEMTs and non-FE MISHEMTs with varying $Al_xGa_{1-x}N$ thickness and Al composition.

The effect of varying $Al_xGa_{1-x}N$ thickness and Al composition on G_m, *SS*, and I_{on} are shown in the Figs. 9(a)–9(c). With the thinning of the $Al_xGa_{1-x}N$ layer in MFSHEMTs, G_m increases in Fig. 9(a) and *SS* decreases in Fig. 9(b) due to the increase of the FE polarization of the FE $HfZrO/Al_2O_3$ gate stack. Moreover, I_{on} decreases with the thinning of the AlGaN layer because of the decrease of the AlGaN polarization in Fig. 9(c). As the Al composition increases, G_m and I_{on} increase due to the inducted more 2DEG. A high gate electric field is required to effectively control the large 2DEG induced by the high Al composition in the channel. Consequently, the *SS* in the device increases with the Al composition. Based on FE $HfZrO/Al_2O_3/Al_xGa_{1-x}N/GaN$ MFSHEMTs and non-FE $HfO_2/Al_2O_3/Al_xGa_{1-x}N/GaN$ MISHEMTs, the difference percentage of G_m, *SS*, and I_{on} are analyzed with varying $Al_xGa_{1-x}N$ thickness and Al composition in Figs. 9(d)–9(f). The difference percentage of G_m and I_{on} increase with decreasing AlGaN thickness, as shown in Figs. 9(d) and 9(f), which is attributed to the enhanced FE polarization in MFSHEMTs. Compared with non-FE MISHEMTs with increasing Al composition, G_m increases and the decrease of I_{on} is effectively inhibited for FE device. The difference percentage of *SS* first increases and then decreases with decreasing AlGaN thickness in Fig. 9(e). As the AlGaN thickness reduces from 20 nm to 10 nm, the degree of 2DEG density decrease is not large, indicating that the FE polarization acting on the abundant 2DEG improves the difference percentage of *SS*. Due to the rapid decline of 2DEG with AlGaN thickness from 10 nm to 3 nm, FE polarization acts on a small number of 2DEG, causing the reduction of the difference percentage of *SS*.

The V_{TH} of the FE $HfZrO/Al_2O_3/Al_xGa_{1-x}N/GaN$ MFSHEMTs with varying AlGaN thickness and Al composition is shown in Fig. 10. Clearly, V_{TH} decreases with decreasing Al composition and AlGaN thickness. When the thickness of the AlGaN layer decreases to a certain extent, the reduction of V_{TH} has fewer with the decrease of Al composition because of the lower 2DEG density. Thus, by controlling the $Al_xGa_{1-x}N$ thickness and composition in FE MFSHEMTs, V_{TH} can be adjusted to afford an enhanced device.

Table 2 summarizes electrical characteristics of G_m, *SS*, I_{on}, and V_{TH} with the various $Al_xGa_{1-x}N$ thickness and Al composition in FE heterostructure $HfZrO/Al_2O_3/AlGaN/GaN$ MFSHEMTs. When the thickness of AlGaN barrier decreases to 3 nm, the Al compositions of 0.15 and 0.35 were compared in electrical properties of FE MFSHEMTs. As the Al composition changes from 0.15 to 0.35, the G_m and I_{on} increase from 101 mS/mm to 234 mS/mm and 429 mA/mm to 727 mA/mm, respectively. Meanwhile, V_{TH} increases only 0.5 V in the Al composition from 0.15 to 0.35, and *SS* increases from 63 mV/dec to 68 mV/dec. As a result, the high Al composition with AlGaN thickness of 3 nm has more advantages with the low Al composition in device characteristics.

Table 2. The electrical characteristics of G_m, *SS*, I_{on}, and V_{TH} with the various $Al_xGa_{1-x}N$ thickness and Al composition in FE heterostructure $HfZrO/Al_2O_3/AlGaN/GaN$ MFSHEMTs.

Al composition		AlGaN thickness				
		20 (nm)	15 (nm)	10 (nm)	7 (nm)	3 (nm)
0.35	G_m (mS/mm)	196	207	214	220	234
	SS (mV/dec)	77	75	72	70	69
	I_{on} (mA/mm)	792	770	758	738	727
	V_{TH} (V)	−6.0	−4.4	−2.8	−1.8	−0.5
0.3	G_m (mS/mm)	178	190	193	195	207
	SS (mV/dec)	76	74	71	69	68
	I_{on} (mA/mm)	682	675	657	649	643
	V_{TH} (V)	−5	−3.7	−2.3	−1.5	−0.4
0.25	G_m (mS/mm)	156	164	170	171	182
	SS (mV/dec)	75	73	70	68	67
	I_{on} (mA/mm)	585	572	557	544	536
	V_{TH} (V)	−4	−2.9	−1.8	−1.2	−0.2
0.2	G_m (mS/mm)	127	132	136	137	148
	SS (mV/dec)	73	70	69	66	64
	I_{on} (mA/mm)	436	417	413	408	406
	V_{TH} (V)	−3.0	−2.2	−1.3	−0.8	−0.1
0.15	G_m (mS/mm)	86	89	92	93	101
	SS (mV/dec)	71	69	67	64	63
	I_{on} (mA/mm)	260	257	256	254	249
	V_{TH} (V)	−2.1	−1.5	−0.9	−0.5	0

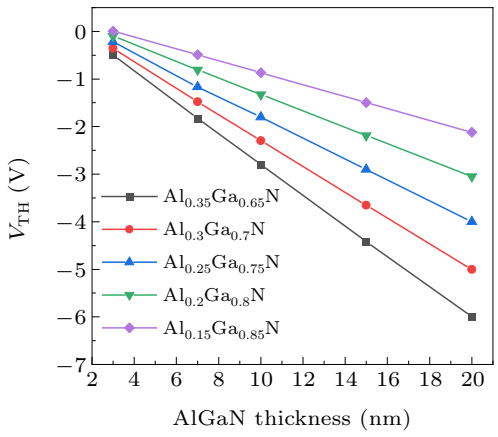


Fig. 10. The V_{TH} curves of FE $HfZrO/Al_2O_3/Al_xGa_{1-x}N/GaN$ MFSHEMTs with varying AlGaN thickness and Al composition.

4. Conclusion

In summary, the effect of the $Al_xGa_{1-x}N$ thickness and Al composition on the electrical properties was analyzed by simulating FE $HfZrO/Al_2O_3/AlGaN/GaN$ MFSHEMTs and non-FE $HfO_2/Al_2O_3/Al_xGa_{1-x}N/GaN$ MISHEMTs. It is found that the 2DEG density of FE $HfZrO/Al_2O_3$ MFSHEMTs exhibits an increase of 30.5%, 58.0%, and 134.3% over that of the non-FE HfO_2/Al_2O_3 gate stack with $Al_{0.25}Ga_{0.75}N$ barrier thicknesses of 20, 10, and 3 nm, respectively. The decrease of the 2DEG density with the thinning of the AlGaN layer is effectively inhibited in FE capacitors compared to that of the non-FE HfO_2/Al_2O_3 gate stack, which is attributed to the increase of the FE

polarization in the $HfZrO/Al_2O_3$ gate stack. Compared to non-FE $HfO_2/Al_2O_3/Al_xGa_{1-x}N/GaN$ MISHEMTs, FE $HfZrO/Al_2O_3/Al_xGa_{1-x}N/GaN$ MFSHEMTs afford enhanced G_m, *SS*, and I_{on}. High Al composition with a 3-nm AlGaN barrier layer has a remarkable effect in the improvement of G_m and I_{on}, stemming from the induced large 2DEG and high FE polarization. Furthermore, *SS* and V_{TH} of FE devices decrease with the reduction of the AlGaN thickness and Al composition, which is beneficial for realizing enhanced devices with high switching performances.

Acknowledgments

Project supported by Guangxi Science and Technology Planning Project (Grant Nos. AD19245066, AA19254015, AD21220150, and AD18281037), the National Nature Science Foundation of China (Grant Nos. 61874036, 62174041, and 62041403), China Postdoctoral Science Foundation (Grant No. 2020M683626XB), the Natural Science Foundation of Guangxi Zhuang Autonomous Region (Grant No. 2018GXNSFAA138025), Guangxi Innovation Research Team Project (Grant No. 2018GXNSFGA281004), GUET Excellent Graduate Thesis (Grant No. YXYJRX01), and the Fund from the State Key Laboratory of ASIC & System (Grant No. KVH1233021).

References

[1] Fletcher A S A and Nirmal D 2017 *Superlattices Microstruct.* **109** 519
[2] Rawat A, Surana V K, Meer M, Bhardwaj N, Ganguly S and Saha D 2019 *IEEE Trans. Electron Dev.* **66** 2557
[3] Sandeep V and Pravin J C 2021 *Superlattices Microstruct.* **156** 106954
[4] Reddy B P K, Teja K B R and Kandpal K 2018 *Semiconductors* **52** 420
[5] Chung J W, Roberts J C, Piner E L and Palacios T 2008 *IEEE Electron Dev. Lett.* **29** 1196
[6] Yue Y, Hao Y, Feng Q, Zhang J, Ma X and Ni J 2008 *Sci. China, Ser. E* **52** 2762
[7] Meng D, Lin S, Wen C P, Wang M, Wang J, Hao Y, Zhang Y, Lau K M and Wu W 2013 *IEEE Electron Dev. Lett.* **34** 738
[8] Sharma A and Roy K 2017 *IEEE Electron Dev. Lett.* **38** 1165
[9] Vasić R, Consiglio S, Clark R D, Tapily K, Sallis S, Chen B, Newby D, Medikonda M, Raja Muthinti G, Bersch E, Jordan-Sweet J, Lavoie C, Leusink G J and Diebold A C 2013 *J. Appl. Phys.* **113** 234101
[10] Saeidi A, Jazaeri F, Stolichnov I and Ionescu A M 2016 *IEEE Trans. Electron Dev.* **63** 4678
[11] Cheng T D, Zhou N J and Li P 2015 *J. Mater. Sci. Mater. Electron.* **26** 7104
[12] Zhu J, Chen L, Jiang J, Lu X, Yang L, Hou B, Liao M, Zhou Y, Ma X and Hao Y 2018 *IEEE Electron Dev. Lett.* **39** 79
[13] Gruverman A, Cao W, Bhaskar S and Dey S K 2004 *Appl. Phys. Lett.* **84** 5153
[14] Senthil Kumar M, Sumathi R R, Giridharan N V, Jayavel R and Kumar J 2002 *Mater. Lett.* **52** 80
[15] Reddy V R, Janardhanam V, Ju J W, Hong H and Choi C J 2014 *Semicond. Sci. Technol.* **29** 075001
[16] Jia S, Li X, Li G, Xie S and Chen Y 2019 *J. Mater. Sci. Mater. Electron.* **30** 9751
[17] Yang S Y, Zhan Q, Yang P L, Cruz M P, Chu Y H, Ramesh R, Wu Y R, Singh J, Tian W and Schlom D G 2007 *Appl. Phys. Lett.* **91** 022909
[18] Yang A, Yao B, Ding Z, Deng R and Li Y 2021 *Mater. Sci. Semicond. Process.* **126** 105659
[19] Niu W, Zhang Y, Gan Y, Christensen D V, Soosten M V, Garcia-Suarez E J, Riisager A, Wang X, Xu Y, Zhang R, Pryds N and Chen Y 2017 *Nano Lett.* **17** 6878
[20] Lomenzo P D, Chung C, Zhou C, Jones J L and Nishida T 2017 *Appl. Phys. Lett.* **110** 232904
[21] Muller J, Boscke T S, Schroder U, Mueller S, Brauhaus D, Bottger U, Frey L and Mikolajick T 2012 *Nano Lett.* **12** 4318
[22] Wu C H, Han P C, Liu S C, Hsieh T E, Lumbantoruan F J, Ho Y H, Chen J Y, Yang K S, Wang H C, Lin Y K, Chang P C, Luc Q H, Lin Y C and Chang E Y 2018 *IEEE Electron Dev. Lett.* **39** 991
[23] Faita F L, Silva J P B, Pereira M and Gomes M J M 2015 *Appl. Phys. Lett.* **107** 242105
[24] Zhang W L, Mao Y H, Cui L, Tang M H, Su P Y, Long X J, Xiao Y G and Yan S A 2020 *Phys. Chem. Chem. Phys.* **22** 21893
[25] Mueller S, Mueller J, Singh A, Riedel S, Sundqvist J, Schroeder U and Mikolajick T 2012 *Adv. Funct. Mater.* **22** 2412
[26] Starschich S, Griesche D, Schneller T, Waser R and Böttger U 2014 *Appl. Phys. Lett.* **104** 202903
[27] Müller J, Schröder U, Böscke T S, Müller I, Böttger U, Wilde L, Sundqvist J, Lemberger M, Kücher P, Mikolajick T and Frey L 2011 *J. Appl. Phys.* **110** 114113
[28] Wang J, Zhou D, Dong W, Yao Y, Sun N, Ali F, Hou X and Liu F 2020 *Ceram. Int.* **46** 22550
[29] Chernikova A G, Kozodaev M G, Negrov D V, Korostylev E V, Park M H, Schroeder U, Hwang C S and Markeev A M 2018 *ACS Appl. Mater. Interfaces* **10** 2701
[30] Schroeder U, Richter C, Park M H, Schenk T, Pesic M, Hoffmann M, Fengler F P G, Pohl D, Rellinghaus B, Zhou C, Chung C C, Jones J L and Mikolajick T 2018 *Inorg. Chem.* **57** 2752
[31] Perevalov T V, Gritsenko V A, Gutakovskii A K and Prosvirin I P 2019 *JETP Lett.* **109** 116
[32] Kim H B, Jung M, Oh Y, Lee S W, Suh D and Ahn J H 2021 *Nanoscale* **13** 8524
[33] Zhang Z, Yu G, Zhang X, Deng X, Li S, Fan Y, Sun S, Song L, Tan S, Wu D, Li W, Huang W, Fu K, Cai Y, Sun Q and Zhang B 2016 *IEEE Trans. Electron Dev.* **63** 731
[34] Fu C, Lin Z, Cui P, Lv Y, Zhou Y, Dai G, Luan C, Liu H and Cheng A 2018 *App.l Phys. A Mater. Sci. Process.* **124** 299
[35] Yue Y, Hao Y, Zhang J, Feng Q, Ni J and Ma X 2008 *Chin. Phys. B* **17** 1405
[36] Wang C, Wei Y C, Tan X, Ali L and Jing C Q 2021 *Mater. Sci. Semicond. Process.* **135** 106038
[37] Chen H, Tang L, Liu L, Chen Y, Luo H, Yuan X and Zhang D 2021 *Appl. Surf. Sci.* **542** 148737
[38] Xu Q, Chen K, Xu G, Xiang J, Gao J, Wang X, Li J, He X, Li J, Wang W and Chen D 2021 *IEEE Trans. Electron Dev.* **68** 3696
[39] Wu J, Kanyang R, Han G, Zhou J, Liu Y, Wang Y, Peng Y, Zhang J, Sun Q Q, Zhang D W and Hao Y 2018 *IEEE Electron Dev. Lett.* **39** 614
[40] Stolichnov I, Malin L, Muralt P and Setter N 2007 *J. Eur. Ceram. Soc.* **27** 4307
[41] Kong Y C, Xue F S, Zhou J J, Li L, Chen C and Li Y R 2008 *Appl. Phys. A Mater. Sci. Process.* **95** 703
[42] Jiang C, Liang R, Wang J and Xu J 2015 *J. Phys. D: Appl. Phys.* **48** 365103
[43] Jang K, Ueyama N, Kobayashi M and Hiramoto T 2018 *IEEE J. Electron Dev.* **6** 346
[44] Hung T H, Krishnamoorthy S, Esposto M, Neelim Nath D, Sung Park P and Rajan S 2013 *Appl. Phys. Lett.* **102** 072105
[45] Li Z and Chow T P 2013 *IEEE Trans. Electron Dev.* **60** 3230
[46] Osipov K, Ostermay I, Bodduluri M, Brunner F, Trankle G and Wurfl J 2018 *IEEE Trans. Electron Dev.* **65** 3176